

# ON-LINE FLOW RATE AND PRESSURE ANALYSIS WITH SENSOR FUSION

David O. Kazmer, Bingfeng Fan, and Ranjan Nageri  
University of Massachusetts Lowell

## Abstract

Plastics injection molding has been limited by the lack of observability and controllability, such that it has not been possible to know or control flow rates and pressures at multiple locations in a mold. An instrumentation and analysis method is presented that allows the estimation of flow rate and pressure at multiple points in an injection mold. While potential improvements are discussed, the presented methods will assist real time process and quality control.

## Introduction

There has been a sustained evolution towards closed loop control in injection molding. Advances are driven largely by economic concerns since machines can typically operate at higher production rates and with high production yields under closed loop control than with open loop control.

Merriam Webster's unabridged dictionary defines closed loop as

Main Entry: **closed loop**

**1** : an automatic control system for an operation or process in which feedback in a closed path or group of paths acts to maintain the output at the desired level

By definition, every closed loop control loop requires a feedback path back to the output being controlled. Most closed loop controls act on feedback regarding machine elements, which do not necessarily provide precise control of the process states that determine the quality of molded products. In fact, with respect to the quality of molded parts, injection molding is not a closed loop process. Instead, injection molding is an open loop process in which many closed loop processes are linked such that the consistency of the molded products is (hopefully) very high.

This paper strives to improve the observability of the injection molding process by 'fusing' information from the molding machine, sensors in the injection mold, and real time flow analysis. As a result, the flow rates and pressures at multiple locations in an injection mold can be estimated and used for real time control. The results are useful in several ways, including but not limited to:

- Estimation of cavity pressure from upstream sensors, which may be more economical or robust than those placed in the mold;
- Estimation of flow rates through multiple branches and gates in a feed system;
- Use of estimated flow rates and pressures for quality control;
- Use of estimated flow rates and pressures for real time process control with adjustable valves, thereby enabling each valve to provide distinct filling and packing stages;
- Use of redundant information to estimate changes in the melt.

This work builds on several past endeavors, including those related to cavity pressure sensing [1-4], sensor fusion [5], on-line rheometry [6], and others. Given space limitations, the reader is provided the references to consult as interested.

The paper progresses as follows. First, the relationships between flow and pressure for generalized Newtonian fluids are presented. Second, a system of equations is developed to model a flow network. Third, the approach is validated against a commercial simulation. Finally, the paper discusses potential improvements.

## Generalized Newtonian Fluids

While the polymer rheology is complex, the Cross-WLF model has been found to provide good fits to experimental data [7]:

$$\eta(\dot{\gamma}, T, P) = \frac{\eta_0(T, P)}{1 + \left(\frac{\eta_0 \dot{\gamma}}{\tau^*}\right)^{1-n}} \quad (1)$$

where  $n$  denotes the power-law index,  $\tau^*$  is a critical stress level at which  $\eta$  is in transition between the Newtonian limit  $\eta_0$  and the power law regime, and  $\dot{\gamma}$  is the shear rate. Some model parameters are shown in Table 1 for a common grade of ABS (GE Plastics' Cyclocac GPM1).

For the purpose of on-line control, it is desirable to find an analytical solution that may be readily evaluated in real time. Such an approach necessarily trades off analysis accuracy for computation speed. For instance, heat transfer from the polymer to the mold, internal viscous generation, pressure dependence, and complex shear-viscosity behaviors may not be adequately modeled in such analytical solutions. However, these and more complex effects can be modeled via numerical algorithms as later discussed.

Analytical solutions have been developed for several generalized Newtonian fluids [8]. For reference, Figure 1 shows the calculated viscosity for the WLF-Cross and several other models at a melt temperature of 253 C. For a Newtonian model, the viscosity is independent of shear rate:

$$\eta = \mu \quad (2)$$

The corresponding relationship between flow rate and pressure is:

$$Q = \frac{\pi R^4 \Delta P}{8 \mu L} \quad (3)$$

where  $P$  is the pressure,  $Q$  is the volumetric flow rate,  $L$  is the length, and  $R$  is the tube radius. Since the viscosity is constant, a Newtonian model will tend to underestimate the viscosity at low shear rates, and overestimate the viscosity at

high shear rates. According, the Newtonian model will be inaccurate unless the process is occurring at low shear rates and the material exhibits a Newtonian plateau, or if a narrow range of shear rates is encountered at which the material has been characterized.

By introducing a second constant, the power-law model provides a straight line relation between the log of the viscosity and the log of shear rate:

$$\eta(\dot{\gamma}) = m\dot{\gamma}^{n-1} \quad (4)$$

where  $m$  is the reference viscosity at a shear rate of 1/sec and  $n$  is the power law index. The corresponding relationship between flow rate and pressure is:

$$Q = \left( \frac{\pi R^3}{s+3} \right) \left( \frac{R\Delta P}{2mL} \right)^s \quad (5)$$

where  $s$  defined as  $1/n$ . Since the model does not include a Newtonian plateau, the power law model tends to overestimate the viscosity at low shear rates, though its accuracy can be improved by characterizing the material across the desired range of shear rates.

By introducing a third constant, the Ellis model provides both a power law and Newtonian regime:

$$\frac{\eta_0}{\eta(\tau)} = 1 + \left( \frac{\tau}{\tau_{1/2}} \right)^{\alpha-1} \quad (6)$$

where  $\tau_{1/2}$  is the shear stress at which the viscosity is 50% of the Newtonian limit,  $\eta_0$ , and  $\alpha-1$  is the slope in the power law regime. The corresponding relationship between flow rate and pressure is:

$$Q = \frac{\pi R^4 \Delta P}{8\eta_0 L} \left[ 1 + \left( \frac{4}{3+\alpha} \right) \left( \frac{R\Delta P}{2L\tau_{1/2}} \right)^{\alpha-1} \right] \quad (7)$$

Table 1 also provides the derived coefficients and average absolute percentage error for the Newtonian, power-law, and Ellis models. It is observed that the error decreases with each added coefficient. Improvements in the rheological modeling are likewise illustrated in Figure 1. Similar sets of formulae have been derived for viscous flow in channels, annuli, and other shapes. It is observed that the complexity of the analytical solutions increases with the complexity of the rheological models.

## Flow Networks

This research is directed to providing estimates of melt flow rates and pressures at varying locations in an injection mold. If the rheology of the material is known, then the analytical solutions may be used to estimate the flow rates from measured pressure drops. Once the flow rates are known, similar methods can be used to estimate the downstream pressures where sensed information may not be readily available.

A flow conductance matrix,  $\mathbf{K}$ , may be used to relate the vector of flow rates,  $\mathbf{Q}$ , to the vector of pressures,  $\mathbf{P}$ :

$$Q_i = K_{ij} P_j \quad (8)$$

As an example, consider the flow network shown in Figure 2. In this example, each flow segment is 50 mm in length with the diameters indicated in Figure 2. If the

Newtonian model is used with a viscosity of 100 PaSec, then this flow network can be modeled as:

$$\begin{bmatrix} Q_1 \\ Q_2 \\ Q_3 \\ Q_4 \\ Q_5 \\ Q_6 \\ Q_7 \end{bmatrix} = \begin{bmatrix} -49.09 & 49.09 & 0 & 0 & 0 & 0 & 0 \\ 49.09 & -90.57 & 20.11 & 20.11 & 0 & 1.26 & 0 \\ 0 & 20 & -40.22 & 0 & 20.11 & 0 & 0 \\ 0 & 20 & 0 & -40.22 & 0 & 0 & 20.11 \\ 0 & 0 & 20.11 & 0 & -20.11 & 0 & 0 \\ 0 & 1.26 & 0 & 0 & 0 & -1.26 & 0 \\ 0 & 0 & 0 & 20 & 0 & 0 & -20.11 \end{bmatrix} \begin{bmatrix} P_1 \\ P_2 \\ P_3 \\ P_4 \\ P_5 \\ P_6 \\ P_7 \end{bmatrix} \quad (9)$$

where the units of flow rate and pressure are cc/sec and MPa, respectively.

Consider a conventional injection molding process where the pressures at the inlet ( $P_1$ ) and each of the gates ( $P_5$ ,  $P_6$ , and  $P_7$ ) are known. In this example, let  $P_1=100$ ,  $P_5=40$ ,  $P_6=70$ ,  $P_7=60$ . It may appear that the solution is undefined since only four pressures are specified from a total of 14 unknowns. In fact, the problem can be solved since conservation of mass requires the net flow rate at points 2, 3, and 4 to be zero and the remaining 7 unknowns are defined by the seven equations provided by the flow conductance matrix. For this example, the solution specifies a flow rate at the inlet of 724 cc/sec, and flow rates at the gates marked 5, 6, and 7 of 452, 20, and 252 cc/sec. For reference, the pressures at points 2, 3, and 4 in the feed system are 85.2, 62.6, and 72.6 MPa, respectively.

Consider the same injection molding example where only the pressures in the feed system at locations 1 to 4 are known with the values of 100, 89, 80, and 75 MPa. This set of information corresponds to that used by the *decoupled gating* process, which is desirable since no instrumentation is installed in the cavity. In this case, the sensor fusion allows for estimation of the flow rates and pressures at the downstream gates labeled 5, 6, and 7 as {180 cc/sec, 71 MPa}, {79 cc/sec, 28 MPa}, and {280 cc/sec, 61 MPa} respectively.

## Validation

The described method was validated against a commercial simulation for the four mold cavity geometries listed in Table 2. Each cavity was located 400 mm from the center of the mold. The hot runner was 12 mm in diameter, with the length of the sprue and drops equal to 200 mm. The predicted filling patterns are shown in Figure 3. A packing phase analysis was also conducted to predict the pack pressures, flow rates, and V/P switchover for each of the cavities. The measured pressures at the inlet, location 5, and the gates, locations 1 to 4, are plotted in Figure 4. It is observed that the pressures in the filling and packing stages are dynamic and difficult to interpret. Specifically, it is not simple to determine what the flow rates to the cavities are, if the cavities have been filled, and what post-filling effects are present. Figure 5 provides the flow rates from the simulation, which are not normally obtainable on-line.

If the Newtonian model is used with a viscosity of 331 Pa Sec, then this flow network can be modeled as:

$$\begin{bmatrix} Q_1 \\ Q_2 \\ Q_3 \\ Q_4 \\ Q_5 \\ Q_6 \end{bmatrix} = \begin{bmatrix} -2.56 & 0 & 0 & 0 & 0 & 2.56 \\ 0 & -2.56 & 0 & 0 & 0 & 2.56 \\ 0 & 0 & -2.56 & 0 & 0 & 2.56 \\ 0 & 0 & 0 & -2.56 & 0 & 2.56 \\ 0 & 0 & 0 & 0 & -7.68 & 7.68 \\ 2.56 & 2.56 & 2.56 & 2.56 & 7.68 & -17.92 \end{bmatrix} \begin{bmatrix} P_1 \\ P_2 \\ P_3 \\ P_4 \\ P_5 \\ P_6 \end{bmatrix} \quad (10)$$

where the units of flow rate and pressure are cc/sec and MPa, respectively. Given this flow conductance matrix and the melt pressures obtained from simulation or actual process measurements, the flow rates through each of the gates can be estimated throughout the molding process.

The results are shown in Figure 6. Given the simplicity of the model, they qualitatively represent the flow rates at each of the gates. For instance, the results clearly show the early filling of cavities 1 and 2, the flow rate surges towards the end of the filling stage in cavity 4, and the flow rate decay during the packing stage for all cavities. However, the results are not quantitatively accurate due to the poor rheological modeling. Since no shear dependence of the viscosity is modeled, this approach grossly underestimates the flow rates to the large cavities.

By including the shear rate dependence of the viscosity in the model, it is expected that the results would be improved. The results for the power law and Ellis models are shown in Figures 7 and 8, respectively. Not surprisingly, the flow rate estimates become more accurate. Consistent with its underlying rheological model, the power law solution now overestimates the flow rates into the small mold cavities (due to shear thinning) but greatly improves the flow rate estimates for the larger cavities. With an additional coefficient, the Ellis solution improves the flow rate estimates by correctly reducing the estimated flow rates to the small cavities while correctly increasing the estimated flow rates to the large cavities towards the end of filling.

However, it is noted that the flow rate behavior for cavity 3, the large square, is not adequately captured. Given that the Ellis model accurately represents the viscosity across a wide shear rate range, rheological modeling is likely not the issue. Instead, it is possible that internal viscous heating due to sustained high shear rates might have caused an increase in the melt temperature in this leg of the feed system. This thesis was verified by the examination of the bulk temperatures provided in Figure 9. For the small cavities, the bulk temperature was uniform. For the large cavities, however, the melt temperature increased by approximately 10 C, which would significantly reduce the melt viscosity and accordingly increase the flow rates. As such, the assumption of isothermal flow may not be adequate for accurate estimation of flow rates.

## Discussion

There are two straightforward approaches for improving the described approach involving 1) on-line rheological modeling, and 2) non-isothermal flow analysis. First, it should be noted that the previous results were achieved purely with the inlet and outlet pressures. By including data regarding the ram displacement, it is possible to cross-check

the estimated flow rates with the observed input flow rate into the cavity. This comparison can be used to estimate the viscosity on-line and thereby improve the flow rate estimates.

Consider that the inlet flow rate should equal the sum of the outlets' flow rates (neglecting melt compressibility, which could be readily included in a numerical treatment). As such, it is a simple matter to adjust the flow rate estimates by correcting for changes in viscosity due to temperature, composition, etc. A very simple correction to ensure conservation of mass would be:

$$Q_{i,corrected} = Q_{i,uncorrected} \frac{Q_{inlet,observed}}{\sum_i Q_{i,uncorrected}} \quad (11)$$

where  $i$  is an index for each of the gates. Applying this approach to the validation example provides the flow rate history shown in Figure 10. Clearly the solution is improved with respect to the flow rate estimates for the larger cavities. Fundamentally, however, this simple correction is not valid. Specifically, such a correction may reduce the accuracy of the flow rate estimates for those systems that have errors which are not distributed equally across all branches of the feed system.

For comparison, Table 3 provides an estimate of the part weight, measured in grams, calculated for each the various models. It is observed that the errors in the estimated flow rates are on the order of 30%. In large part, this magnitude of error is due to the variation in the part geometries and the shear heating in the feed system leading to the larger cavities. Smaller errors would be expected for more conventional molding operations.

To further improve the flow rate estimates, a non-isothermal flow analysis can be developed. The heat transfer in a tubular feed system including heat conduction, heat convection, and viscous dissipation is:

$$\rho C_p \left( \frac{\partial T}{\partial t} + u \frac{\partial T}{\partial l} \right) = \frac{1}{r} \frac{\partial}{\partial r} \left( rk \frac{\partial T}{\partial r} \right) + \eta \dot{\gamma}^2 \quad (12)$$

The solution of this energy equation and the appropriate mass and momentum equations for a flow network can be conducted in real time for a reasonable number of elements (for example, dozens of elements along the length of the feed system with several optimally spaced layers in the radial direction). Given that the flow conductance matrix is symmetric, efficient solution strategies can be employed to reduce the computational burden. With continuing increases in computing speed, the capability and resolution of the implemented analyses will only improve.

## Conclusions

The described principles of polymer processing are sufficient for flow rate and pressure estimation using a fusion of sensed information. While the results are not perfect and significant issues have been raised, the described approach for estimating flow rates and pressures is a significant and enabling advancement for real time process and quality control. For the first time, the described methods allow the flow rate to be specified and controlled on a gate by gate basis. Moreover, the same approach allows the

cavity pressure to be estimated by measuring the pressure at remote locations, which thereby avoids costly and sometimes impossible mold modifications.

Continued work will implement the improvements discussed in this paper in an on-line system, and verify the added benefits in practical injection molding operations.

### Acknowledgements

This work was funded under grant number #0245309 from the Materials Processing & Manufacturing Program of the National Science Foundation. This work does not represent the opinions of the National Science Foundation.

### Bibliography

- [1] J. W. Mann, "Process Parameter Control: the Key to Optimization," *Plastics Engineering*, vol. 30, pp. 25-27, 1974.
- [2] M. R. Kamal, W. I. Patterson, N. Conley, D. Abu Fara, and G. Lohfink, "Dynamics and Control of Pressure in the Injection Molding of Thermoplastics," *Polymer Engineering and Science*, vol. 27, pp. 1403-1410, 1987.
- [3] F. Gao, I. A. N. Patterson, and M. R. Kamal, "Self-tuning cavity pressure control of injection molding filling," *Advances in Polymer Technology*, vol. 13, pp. 111-120, 1994.
- [4] S. L. B. Woll and D. J. Cooper, "Pattern-based closed-loop quality control for the injection molding process," *Polymer Engineering and Science*, vol. 37, pp. 801-812, 1997.
- [5] L.-J. Chien, C. L. Thomas, and D. R. Lawson, "Sensor/model fusion for improved process understanding and control in injection molding," presented at CAE and Intelligent Processing of Polymeric Materials, Dallas, TX, 1997.
- [6] P. D. Coates, A. R. Haynes, and R. G. Speight, "In-line characterization of polymer deformation in melt and solid phase processing," *Polymer*, vol. 35, pp. 3831-3843, 1994.
- [7] M. M. Cross, *Rheological Acta*, vol. 18, pp. 609, 1979.
- [8] Z. Tadmor and C. G. Gogos, *Principles of Polymer Processing*: John Wiley & Sons, 1979.

Table 1: Rheological models and average absolute errors

Model	AAE	Coefficient	Value
Cross-WLF	N/A	$n$	0.306
		$\tau^*$	66057
		$D_1$	1.06E+13
		$D_2$	373.15
		$D_3$	0
		$A_1$	30.5
Newtonian	212.5	$\mu$	331
Power Law	53.6	$m$	1040
		$n$	0.72
Ellis	14.4	$\eta_0$	621.9
		$\tau_{1/2}$	40324
		$\alpha-1$	1.40

Table 2: Mold geometries for validation

Cavity	Geometry
1	200 mm by 50 mm rectangle, end-gated, 2 mm thick
2	300 mm by 50 mm rectangle, edge-gated 100 mm from end, 2 mm thick
3	400 mm by 400 mm square, center gated, 3 mm thick
4	Two cascading right triangles, 150 mm in height, edge gated, 3 mm thick

Table 3: Comparison of part weight estimates

Model	1	2	3	4
Actual	22.0	32.9	542.5	577.3
Newtonian	24.8	34.4	167.0	230.5
Power Law	34.9	52.9	372.3	494.7
Ellis	29.5	43.4	318.9	434.1
Ellis, Corrected	30.5	45.5	453.2	638.1

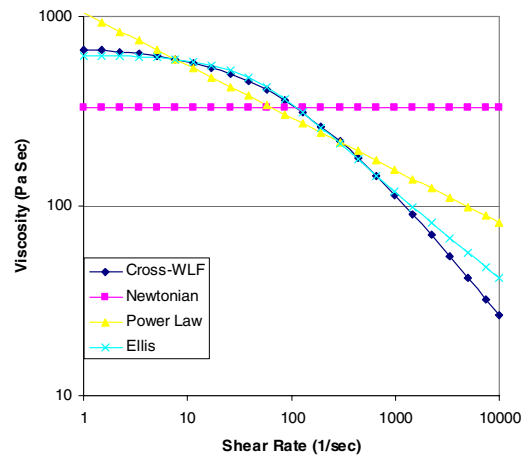


Figure 1: Shear rate-viscosity models for ABS

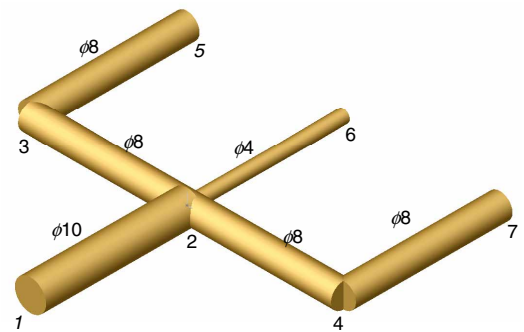


Figure 2: Flow network

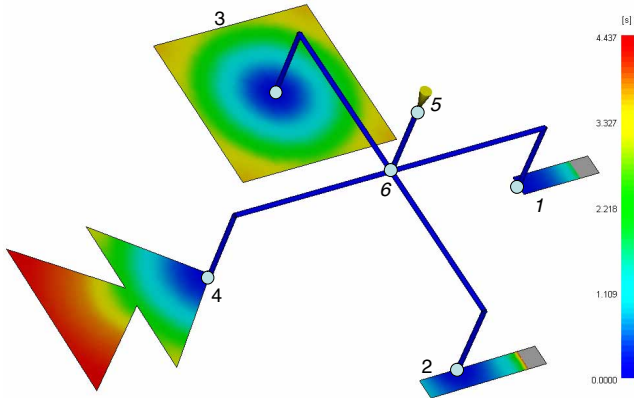


Figure 3: Filling patterns

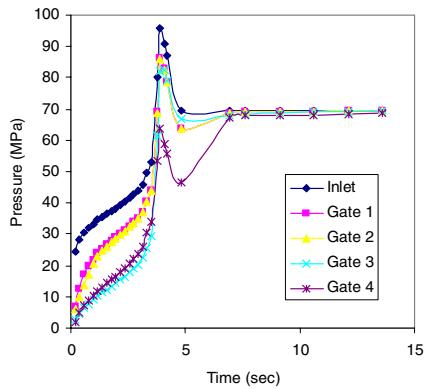


Figure 4: Observed melt pressures

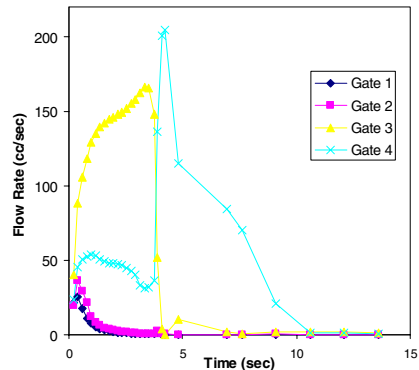


Figure 5: Observed melt flow rates

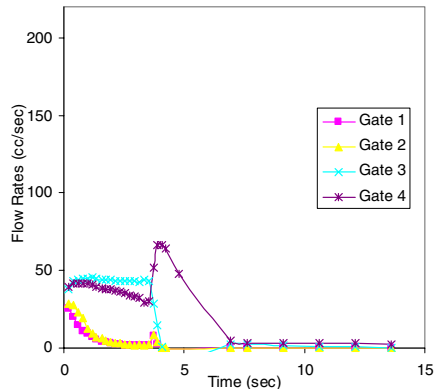


Figure 6: Predicted melt flow rates according to Newtonian model

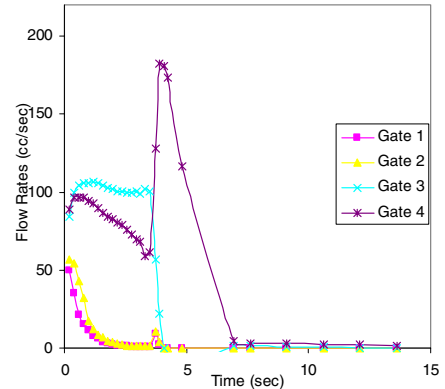


Figure 7: Predicted melt flow rates according to Power Law model

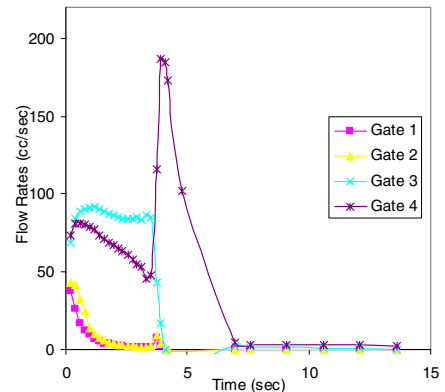


Figure 8: Predicted melt flow rates according to Ellis model

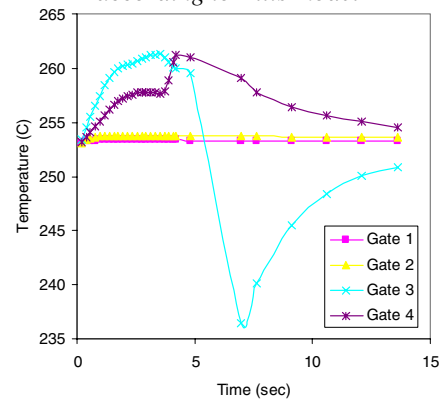


Figure 9: Bulk temperatures in feed system branches

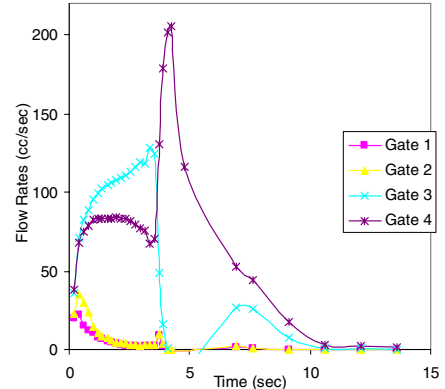


Figure 10: Predicted melt flow rates according to Ellis model corrected for conservation of mass